의학과 석사 학위논문

Prediction of liver regeneration after living donor liver transplantation in the recipients using preoperative CT texture analysis and clinical features

수술 전 간 공여자 CT 영상의 텍스처 분석 및 임상 지표를 이용한 간이식 수술 후 간 수여자의 간 용적 재생 예측

2020년 2월

서울대학교 대학원

의학과 영상의학전공

박정환

Abstract

Prediction of liver regeneration after living donor liver transplantation in the recipients using preoperative CT texture analysis and clinical features

Junghoan Park
Department of Radiology, College of Medicine
The Graduate School
Seoul National University

Objectives

To predict the rate of liver regeneration in recipients after living donor liver transplantation (LDLT) using preoperative CT texture and shape analysis of the future graft and clinical features.

Methods

102 donor-recipient pairs who underwent LDLT using right lobe grafts were retrospectively included for this study. All donors underwent preoperative liver CT using a single CT scanner. We semi-automatically segmented the right lobe of the liver which was

to be a future graft using commercially available software. The volume of the future graft (V_{pre}) was measured, and texture and shape analyses of the V_{pre} were performed. All recipients underwent follow-up CT between 9 and 15 months after surgery. The graft liver was segmented in the same manner, and the volume of the graft (V_{post}) was measured. The regeneration index (RI) was defined by the following equation: $[(V_{post}-V_{pre})/V_{pre}]\times100$ (%). We performed a stepwise, multivariate linear regression analysis to investigate the association between clinical features, texture and shape parameters and RI and to make the best-fit model for predicting RI. The model was also made in the subgroup analysis according to estimated graft-to-receipient weight ratio before transplantation ($eGRWR_{pre}$).

Results

The mean RI was 47.5±38.6%. In univariate analysis, the V_{pre}, energy, effective diameter, surface area, sphericity, $roundness_m$, compactness1, and grey-level co-occurrence matrix (GLCM) contrast were significantly correlated with the RI ($p<0.05$). In multivariate analysis, the effective diameter and $roundness_m$ as well as donor sex, recipient body surface area (rBSA) and white blood cell count (rWBC) were shown to be independent predictors of the RI ($p<0.05$). The best-fit predictive model for the RI was as follows: expected RI (%) = 127.020 – 0.367×effective diameter – 1.827×roundnessm + 47.371×rBSA (m^2) + 12.041×log(rWBC) ($\times 10^3/\mu L$) + 18.034 (if the donor was female). In the subgroup analysis, $eGRWR_{pre}$, $roundness_m$ and kurtosis were shown to be independent predictors of the RI in the larger $eGRWR_{pre}$ group (n=77), while energy and LV_{pre} were the only significant independent predictors of the RI in the smaller $eGRWR_{pre}$ group (n=25).

Conclusions

Clinical features and CT texture parameters of the liver including roundness$_m$ were associated with liver regeneration. Preoperative CT texture analysis of future grafts can be useful for predicting liver regeneration in recipients after LDLT.

Keywords

Liver, Liver transplantation, Liver regeneration, Computed tomography, Texture analysis

Student Number: 2018-25218

Contents

List of Tables and Figures

smaller and larger $eGRWR_{pre}$ subgroups

Table 10. Multivariate linear regression model for predicting RI in the larger $eGRWR_{pre}$ subgroup.

Table 11. Multivariate linear regression model for predicting RI in the smaller $eGRWR_{pre}$ subgroup.

Figure 1. Study diagram for patient inclusion

Figure 2. Schematic example of the segmentation of the liver. (a) Preoperative CT images of a 51-year-old male donor were loaded into the software. (b) The images were processed using an iteration method to decrease noise. (c-e) The radiologist manually drew several ROIs (c) within the liver (red), (d) outside of the liver (blue), (e) within the portal vein, hepatic vein and inferior vena cava (green) with the help of the "HU threshold" function. (f) The software automatically segmented the liver (pink) by expanding (c) to the boundary of the liver while excluding (d) and (e).

Figure 3. Schematic example of the segmentation of the future graft. (a) The segmented liver (pink) on figure 2. (b) Axial and (c) oblique sagittal view of the virtual surgical plane (red line), which was manually drawn by the radiologist. (d) The software automatically segmented the future graft by the virtual surgical plane (pink).

Figure 4. Histogram distribution of the regeneration index (RI). The patients were divided into lower (n = 63) and higher RI groups (n = 39) with a cutoff value of 50%.

Figure 5. Representative cases of (a-c) lower and (d-f) higher RI groups. (a) A preoperative CT image of a 53-year-old male donor who donated liver to a 60-year-old male recipient who had HBV-related HCC. (b) A future graft was segmented and texture and shape features of the future graft were calculated. Estimated RI was calculated to 18.7% by effective diameter (562.3) and $roundness_m$ (5.760). (c) Postoperative CT of the recipient was taken 12 months after LDLT and the transplanted was segmented. RI was finally calculated to 19.2%. (d) Another preoperative CT image of a 25-year-old male donor who donated liver to a 52-year-old male recipient who had HBV-related HCC. (b) Estimated RI was calculated to 80.9% by effective diameter (451.3) and $roundness_m$ (-8.179) in the same manner. (c) Postoperative CT of the recipient was taken 12 months after LDLT and RI was finally calculated to 76.4%.

Introduction

Liver transplantation is the ultimate treatment for end-stage liver disease, and the number of liver transplantations has been increasing rapidly over the last decade [1; 2]. In Korea, there is great demand for liver transplantation because of high prevalence of hepatitis B virus (HBV) infection and associated liver cirrhosis (LC) and hepatocellular carcinoma (HCC), while the rate of deceased organ donation is low. Therefore, liver transplantation in Korea mostly relied on live donors and more than 80% of liver transplantation in adults is living donor liver transplantation (LDLT) [1].

The first successful adult-to-adult LDLT was reported by the Shinshu group in 1994 using the left lobe of the liver as a graft [3]. However, LDLT using the left lobe graft had a major limitation that the size of the graft may be inadequate and may not meet the metabolic demand of a recipient [4; 5]. The advances in LDLT using the right lobe have overcome the restriction of graft size, and therefore, right lobe graft was used in most LDLT in recent years [1]. However, although LDLT using the right lobe are generally considered to be safe [6; 7], donor safety remains a major concern in LDLT using the right lobe especially when the remnant liver volume is smaller than 30 – 35% of total liver volume [8; 9]. Thus, ensuring donor safety as well as the recovery of the recipient liver function is critically important when planning LDLT using the right lobe.

Preoperative contrast-enhanced CT is important for planning of LDLT. Preoperative CT of the donor is used to determine suitability for LDLT and establish a surgical plan by identifying hepatic anatomy and the presence of liver disease and by assessing liver volumetry [10]. However, CT images contain data beyond gross anatomy that are difficult to quantify with the human eye. CT texture analysis (CTTA) is a part of

the growing field of radiomics that provides quantification of the spatial distribution of voxel gray levels in images to mainly analyze spatial heterogeneity [11; 12]. There are various methods applied in the texture analysis including statistical-, model-, and transform-based methods, but statistical-based methods have been most commonly used for the texture analysis. The statistical-based methods derive from the frequency of occurrence of different gray levels, and are further classified into first-, second-, and higher-order statistics. First-order statistics derive from the gray-level frequency histogram. These statistics are simple but do not have information of spatial interrelationship between gray values. Second- or higher-order statistics using gray-level co-occurrence matrix (GLCM, second-order), run-length matrix (RLM, second-order), or neighborhood gray-tone-difference matrix (NGTDM, higher-order), on the other hand, can analyze spatial interrelationship between two or more pixels. Thus, first-order statistics are often supplemented by second- or higher- order statistics [11-13]. Shape features, which are based on the shape of ROI, are not true "texture features" but have often been analyzed together and yielded several significant results [14; 15]. CTTA has mainly been applied in oncology including lesion characterization and pre-treatment and post-treatment assessment [12]. However, there have been several emerging nononcologic applications of CTTA. Liver is one of the frequently-studied organs using CTTA, and there have been studies using CTTA to assess hepatic fibrosis [16; 17] or to predict the risk for hepatic failure after hepatectomy [18]. In addition, CTTA may have potential for predicting liver regeneration in living donor after LDLT [19]. However, to our knowledge, there have been no previous studies on the relationship between liver regeneration after LDLT and CTTA in recipients.

Liver regeneration is a key component for successful LDLT [20], especially with trend of using even small-for-size graft as a candidate of LDLT [21]. Although graft size has been shown to be an important factors affecting liver regeneration, there are numerous other factors that affect liver regeneration including ischemic injury, immunosuppression, steatosis and donor age, although mild steatosis has been reported not to impair the hepatic regeneration power [22-24]. Thus, it would be helpful for surgical planning if we could precisely predict the rate of liver regeneration in the recipient before LDLT using preoperative CT along with other clinical data. Therefore, the purpose of our study was to predict the rate of liver regeneration in recipients after LDLT using clinical features and texture analysis of the future graft on preoperative liver CT.

Materials and Methods

Patients

The institutional review board of our hospital approved this study and the requirement for informed consent was waived due to the retrospective nature of the study.

A total of 220 donor-recipient pairs who underwent LDLT from January 2010 to December 2011 were initially searched for this study. After excluding donor-recipient pairs according to the exclusion criteria shown on Figure 1, 102 donor-recipient pairs (donor, male: female = 76: 26; mean age, 30.4±10.4 years; recipient, male: female = 80: 22; mean age, 53.7±7.0 years) who underwent LDLT using a right lobe graft were included.

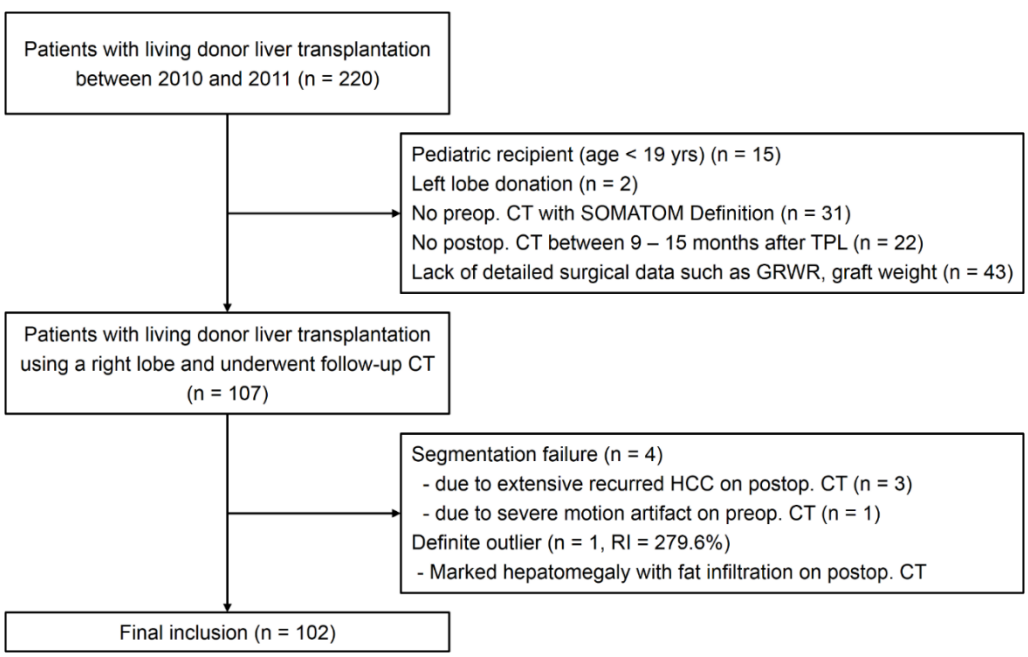

Figure 1. Study diagram for patient inclusion

Among the 102 donor-recipient pairs, three underwent urgent LDLT due to acute hepatic failure (hepatitis B in two, toxic hepatitis in one), and others underwent elective LDLT due to LC and/or HCC. The etiology of LC was variable, but most recipients (72/99 recipients, 73.7%) had HBV-related LC. Other etiologies of LC were as follows: hepatitis C virus (HCV) in eleven, alcohol in ten, combined alcohol and HBV in one, biliary etiology in three, Budd-Chiari syndrome in one, and unknown etiology in one. Sixty-four recipients (62.7%) had HCC at the time of the LDLT.

Preoperative CT acquisition

All donors underwent contrast-enhanced liver CT examination using a single CT scanner (Somatom Definition, Siemens Healthcare) before LDLT. The median interval between the preoperative CT scan and LDLT was 17 days (range, 2 – 166 days). The CT examination included three phases – precontrast, arterial phase and portal phase. For contrast enhancement, 1.5 mL/kg of nonionic contrast material was administered by an automated power injector at a rate of 3.0 mL/s. Arterial phase images were obtained at 19 seconds after the maximum HU of the descending thoracic aorta reached 100 HU using the bolus tracking method, and portal phase images were obtained at 33 seconds after obtaining the arterial phase images. All CT examination was performed using the dual energy mode with following scan parameters: collimation, 14×1.2 mm, tube voltage, 80 and 140 kVp; tube current, automatic tube current modulation; pitch, 0.85; rotation time, 0.5 second, matrix, 512×512; slice thickness, 3 mm; reconstruction interval, 2 mm. All images were reconstructed with an iterative algorithm (Iterative Reconstruction in Image Space (IRIS), Siemens Healthcare) using a soft convolution kernel (D30f).

CT liver volumetry and texture analysis

We used commercially available software (MEDIP, MEDICAL IP) to perform the texture analysis. The portal phase images of the preoperative CT examination of the donors acquired at 140 kVp were used for the texture analysis.

First, semi-automatic segmentation of the right lobe of the liver which was to be a future graft was performed by one radiologist (Junghoan Park, with four years of abdominal CT clinical experience). After loading the CT images into the software, the images were processed using an iteration method to decrease noise. Next, the radiologist manually drew ROIs in a few selected slice images as follows – 1) within the liver, 2) outside of the liver and 3) within the portal vein, hepatic vein and inferior vena cava. When drawing 2) and 3), the radiologist was assisted by the "HU threshold" function, which automatically drew all areas within the range of the specific HU defined by the radiologist. Then, the software automatically segmented the liver by expanding 1) to the boundary of the liver while excluding 2) and 3) to include only the hepatic parenchyma (Figure 2).

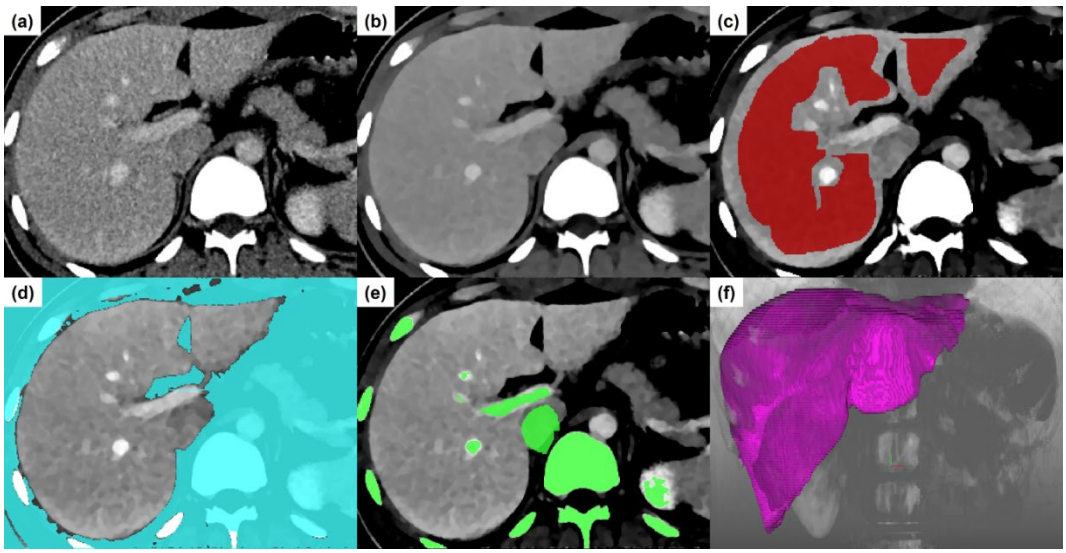

Figure 2. Schematic example of the segmentation of the liver. (a) Preoperative CT images of a 51-year-old male donor were loaded into the software. (b) The images were processed using an iteration method to decrease noise. (c-e) The radiologist manually drew several ROIs (c) within the liver (red), (d) outside of the liver (blue), (e) within the portal vein, hepatic vein and inferior vena cava (green) with the help of the "HU threshold" function. (f) The software automatically segmented the liver (pink) by expanding (c) to the boundary of the liver while excluding (d) and (e).

After segmenting the liver, the radiologist drew a virtual surgical plane between the right and left lobes of the liver with reference to the operative record and the postoperative CT images of the recipients, with particular attention to whether the middle hepatic vein was included in the graft. Then, the software automatically segmented the future graft by the virtual surgical plane (Figure 3). Next, the software automatically calculated the volume of the future graft (LV_{pre}), and the estimated graft-to-recipient weight

ratio ($eGRWR_{pre}$) was manually calculated by dividing LV_{pre} into the recipient weight. Finally, the software calculated a total of 15 texture parameters of the future graft including histogram-based 1st order statistics and GLCM textures as well as eight shape parameters.

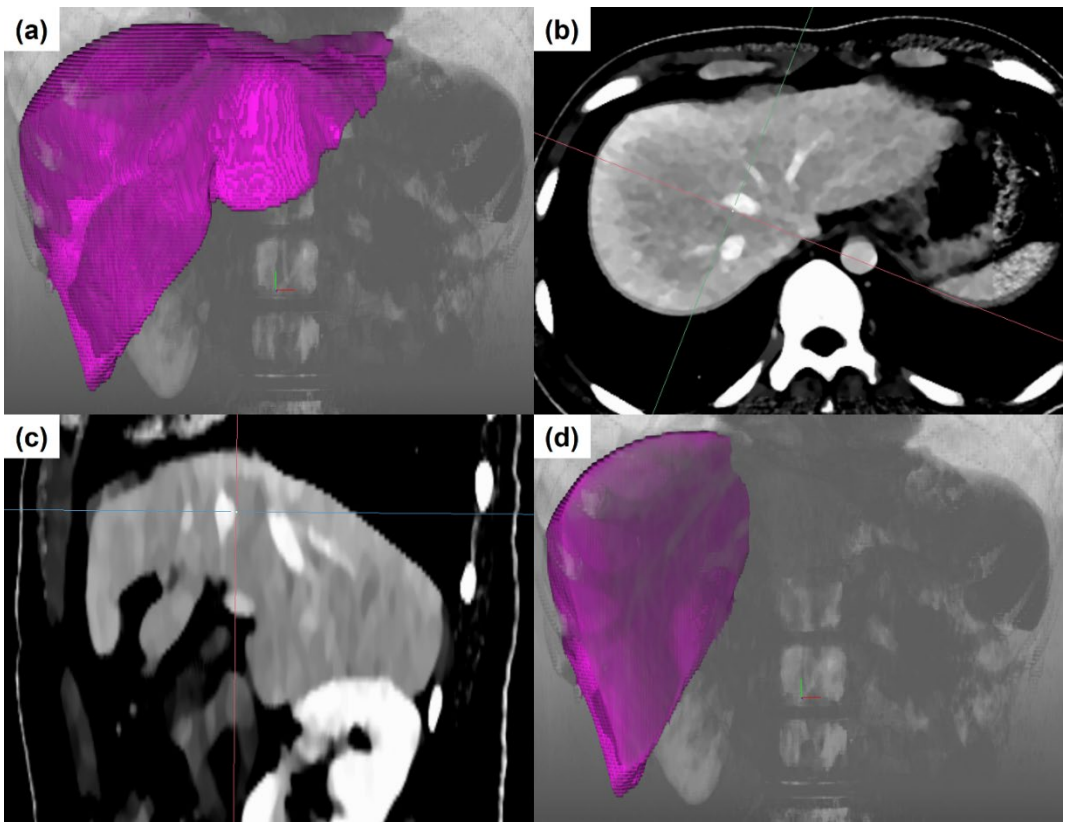

Figure 3. Schematic example of the segmentation of the future graft. (a) The segmented liver (pink) on figure 2. (b) Axial and (c) oblique sagittal view of the virtual surgical plane (red line), which was manually drawn by the radiologist. (d) The software automatically segmented the future graft by the virtual surgical plane (pink).

Postoperative CT acquisition and CT liver volumetry

Due to the retrospective nature of the study, the timing and the protocol used in the postoperative CT of the recipients were varied. We used the CT images of the recipients performed between 9 and 15 months (median, 361 days) after LDLT and at the portal phase to calculate the volume of the transplanted liver (LV_{post}) in the recipient. If there were more than one portal-phase CT images scanned between 9 and 15 months after LDLT, we selected the images which were performed nearest to one year after LDLT.

The transplanted liver was semi-automatically segmented with the software in the same manner as the segmentation of the future graft. After segmentation of the transplanted liver, the LV_{post} was automatically calculated, and estimated graft-to-recipient weight ratio at postoperative follow-up ($eGRWR_{post}$) was calculated by dividing LV_{post} into the recipient weight. With these calculated volumetric parameters, we calculated the regeneration index (RI) for each donor-recipient pair, which was defined by the following equation: $[(LV_{post}-LV_{pre})/LV_{pre}]\times100$ (%).

Statistical analysis

Student's T-test, chi-square test or Fisher's exact test was used to compare the clinical, texture and shape parameters between lower and higher RI groups and between smaller and larger $eGRWR_{post}$ groups according to the variables to be compared. The cutoff value of 2%, which corresponded to the theoretical liver volume, was used for dividing between smaller and larger $eGRWR_{post}$ groups [25]. Univariate linear regression analysis between these parameters and the RI was performed to find the potential predictive variables for the RI. Stepwise multivariate linear regression analysis was performed to investigate the association between clinical, texture and shape parameters and the RI and

to make the best-fit model for predicting the RI. Variables with p-values less than 0.2 in the univariate linear regression analysis were used for the multivariate analysis. Among the group of variables that showed high correlation between the variables, one variable in each group was selected. The prediction model was also made in the subgroup with smaller and larger $eGRWR_{pre}$ with the cutoff value of 1%. A two-sided p-value less than 0.05 was considered statistically significant for all statistical analyses. All statistical analyses were performed using SPSS version 25.0 (IBM Corp.) and SAS version 9.4 (SAS Institute Inc.).

Results

There was no operation-related mortality. Twenty-five recipients (24.3%) experienced postoperative complications. Most of the complications (21/25, 84.0%) were biliary complications that required percutaneous or endoscopic biliary intervention. Other complications were as follows: thrombotic occlusion of hepatic artery, combined disruption of the anastomosis site of hepatic artery and biliary stricture, portal venous stricture, and hepatic venous stricture, all of which required percutaneous intervention and/or reoperation.

The mean graft weight was 748±159 g, and the mean graft-to-recipient weight ratio (GRWR) was 1.18±0.28%. The mean LV_{pre} and LV_{post} were 781±143 mL and 1,120±237 mL, respectively, and the mean $eGRWR_{pre}$ and $eGRWR_{post}$ were 1.22±0.28% and 1.73±0.39%, respectively. The mean RI was 47.5±38.6%, but it was highly variable, ranging from -10.5% to 153.9%. When dividing recipients into lower and higher RI groups with a cutoff value of 50%, there were 63 and 39 recipients in the lower and higher RI groups, respectively (Figure 4). Recipients in the higher RI groups had significantly smaller LV_{pre} (837±121 mL vs. 690±128 mL, $p<0.001$) and $eGRWR_{pre}$ (1.32±0.26% vs. 1.06±0.25%, $p<0.001$), and larger LV_{post} (1,017±158 mL vs. 1,286±251 mL, $p<0.001$) and $eGRWR_{post}$ (1.59±0.25% vs. 1.97±0.46%, $p<0.001$).

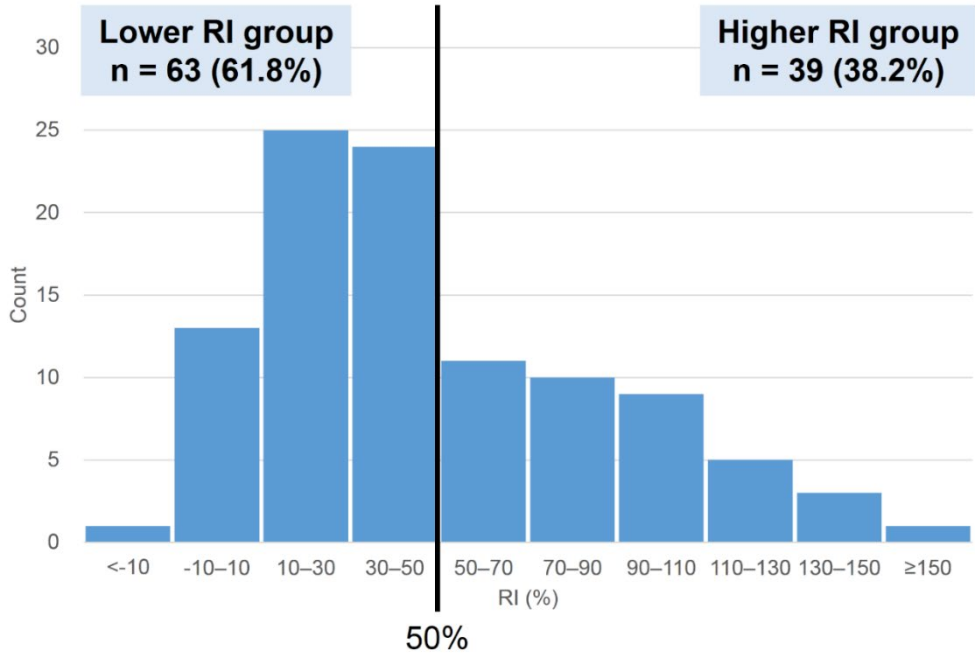

Figure 4. Histogram distribution of the regeneration index (RI). The patients were divided into lower (n = 63) and higher RI groups (n = 39) with a cutoff value of 50%.

Clinical findings and texture features predicting liver regeneration

The comparisons of the clinical, texture and shape parameters between lower and higher RI groups are summarized in Tables 1 and 2, respectively. Since roundness was mostly close to 0.780, we converted roundness to $roundness_m$ as follows to clearly demonstrate the difference between patients: $roundness_m = (roundness–0.780)\times1000$.

Table 1. The comparisons of clinical parameters between lower and higher RI groups

Variables	Total (n = 102)	Lower RI (n = 63)	Higher RI (n = 39)	P-value
Demographics				
Age, donor (years)	30.4 ± 10.4	29.0 ± 9.3	32.7 ± 11.7	0.098
Female sex, donor	26 (25.5%)	8 (12.7%)	18 (46.2%)	< 0.001
Age, recipient (years)	53.7 ± 7.0	54.2 ± 6.7	52.9 ± 7.5	0.352
Female sex, recipient	22 (21.6%)	19 (30.2%)	3 (7.7%)	0.007
Height, recipient (cm)	165.4 ± 7.1	164.6 ± 7.9	166.6 ± 5.5	0.125
Body weight, recipient (kg)	65.6 ± 10.0	65.0 ± 10.3	66.6 ± 9.5	0.418
BMI, recipient (kg/m^2)	24.0 ± 3.2	24.0 ± 3.4	24.0 ± 3.0	0.990
BSA, recipient (m^2)†	1.732 ± 0.154	1.719 ± 0.161	1.752 ± 0.142	0.294
Clinical features, recipient				
Urgent transplantation	3 (2.9%)	2 (3.2%)	1 (2.6%)	1.000
Underlying HCC	64 (62.7%)	40 (63.5%)	24 (61.5%)	0.843
Pretreatment encephalopathy	21 (20.6%)	10 (15.9%)	11 (28.2%)	0.134
Preop. lab findings, recipient				
WBC (× 10^3/μL)	4.42 ± 2.75	3.89 ± 1.99	5.28 ± 3.52	0.029
Hemoglobin (g/dL)	11.4 ± 2.2	11.5 ± 2.3	11.3 ± 1.9	0.675
Platelet (× 10^3/μL)	82.3 ± 48.8	76.2 ± 40.8	92.2 ± 58.7	0.142
Cholesterol (mg/dL)	111.3 ± 42.5	110.8 ± 41.9	112.0 ± 44.1	0.896
Protein (g/dL)	6.57 ± 0.74	6.44 ± 0.75	6.77 ± 0.70	0.030
Albumin (g/dL)	3.07 ± 0.66	3.07 ± 0.67	3.07 ± 0.65	0.950
Total bilirubin (mg/dL)	5.51 ± 8.11	4.71 ± 7.59	6.79 ± 8.82	0.208
Direct bilirubin (mg/dL)	2.66 ± 4.97	2.05 ± 4.26	3.68 ± 5.93	0.206
Alkaline phosphatase (IU/L)	118.9 ± 82.9	115.7 ± 60.7	124.2 ± 110.6	0.614
AST (IU/L)	66.3 ± 51.6	67.3 ± 51.8	64.7 ± 51.9	0.807
ALT (IU/L)	45.3 ± 34.9	48.7 ± 36.1	39.9 ± 32.6	0.218
GGT (IU/L)	65.1 ± 64.0	59.8 ± 56.7	74.4 ± 75.2	0.317

PT-INR	1.67 ± 0.93	1.62 ± 0.97	1.74 ± 0.88	0.532
Creatinine (mg/dL)	1.11 ± 1.10	0.88 ± 0.31	1.48 ± 1.69	0.035
Sodium (mmol/L)	136.3 ± 6.4	136.5 ± 6.2	135.9 ± 6.9	0.641
MELD score	17.3 ± 9.5	16.2 ± 8.5	19.2 ± 10.7	0.144

Note - RI = regeneration index, BMI = body mass index, BSA = body surface area, WBC = white blood cell, AST = aspartate aminotransferase, ALT = alanine aminotransferase, GGT = gamma-glutamyl transferase, PT-INR = prothrombin time-international normalized ratio, MELD = model for end-stage liver disease.

† BSA was calculated according to Mosteller formula: BSA (m^2) = (Height (cm)*Body weight (kg)/3600)$^{1/2}$

Table 2. The comparisons of texture and shape parameters between lower and higher RI group

Variables	**Total (n = 102)**	**Lower RI (n = 63)**	**Higher RI (n = 39)**	**P-value**
Liver volume				
LV_{pre} (mL)	781 ± 143	837 ± 121	690 ± 128	< 0.001
$eGRWR_{pre}$ (%)	1.22 ± 0.28	1.32 ± 0.26	1.06 ± 0.25	< 0.001
LV_{post} (mL)	1120 ± 237	1017 ± 158	1286 ± 251	< 0.001
$eGRWR_{post}$ (%)	1.73 ± 0.39	1.59 ± 0.25	1.97 ± 0.46	< 0.001
1st order statistics				
Mean attenuation (HU)	106.4 ± 8.7	106.1 ± 9.9	107.1 ± 6.5	0.525
Minimum attenuation (HU)	67.2 ± 9.1	67.7 ± 9.3	66.4 ± 8.9	0.478
Maximum attenuation (HU)	148.9 ± 10.4	148.6 ± 11.1	149.4 ± 9.3	0.711
Standard deviation	8.201 ± 1.266	8.234 ± 1.071	8.148 ± 1.544	0.764
Variance	68.84 ± 19.12	68.92 ± 15.83	86.72 ± 23.72	0.963

Skewness	0.929 ± 0.422	0.974 ± 0.379	0.856 ± 0.480	0.173
Kurtosis	1.833 ± 1.089	1.746 ± 0.932	1.973 ± 1.306	0.309
Entropy	4.866 ± 0.245	4.875 ± 0.215	4.851 ± 0.290	0.625
Homogeneity ($\times 10^{-3}$)	9.801 ± 0.909	9.861 ± 1.041	9.704 ± 0.641	0.347
Uniformity ($\times 10^{-3}$)	45.68 ± 8.99	45.22 ± 8.00	46.43 ± 10.47	0.510
Energy ($\times 10^{9}$)	10.52 ± 2.44	10.85 ± 2.63	9.97 ± 2.00	0.075
Geometric features				
Effective diameter	496.5 ± 45.2	514.9 ± 37.1	466.8 ± 41.5	< 0.001
Surface area ($\times 10^{3}$)	89.26 ± 11.04	93.00 ± 8.89	83.21 ± 11.58	< 0.001
Sphericity	0.769 ± 0.084	0.754 ± 0.081	0.793 ± 0.084	0.021
Discrete compactness	0.938 ± 0.021	0.935 ± 0.020	0.942 ± 0.023	0.145
Roundness$_m$	-0.002 ± 5.675	1.261 ± 4.981	-2.044 ± 6.179	0.004
Moment	1.064 ± 0.174	1.058 ± 0.196	1.074 ± 0.133	0.629
Compactness 1	219.7 ± 26.3	229.6 ± 23.4	203.5 ± 22.8	< 0.001
Compactness 2	0.098 ± 0.018	0.100 ± 0.018	0.095 ± 0.018	0.220
2nd order statistics (GLCM)				
GLCM ASM ($\times 10^{-3}$)	11.91 ± 4.66	11.88 ± 4.10	11.96 ± 5.49	0.933
GLCM IDM	0.597 ± 0.056	0.603 ± 0.049	0.589 ± 0.065	0.230
GLCM contrast	132.0 ± 37.1	127.4 ± 21.0	139.4 ± 53.4	0.114
GLCM entropy	7.732 ± 0.482	7.717 ± 0.418	7.756 ± 0.576	0.694
RI (%)	47.5 ± 38.6	22.3 ± 15.6	88.4 ± 28.0	< 0.001

Note - RI = regeneration index, LV_{pre} = volume of the future graft, $eGRWR_{pre}$ = estimated graft-to-recipient weight ratio before transplantation, LV_{post} = volume of the transplanted liver, $eGRWR_{post}$ = estimated graft-to-recipient weight ratio at postoperative follow-up, GLCM = grey level co-occurence matrix, ASM = angular second moment, IDM = inverse difference moment.

There were more female donors (46.2% vs. 12.7%, p<0.001) and fewer female recipients (7.7% vs. 30.2%, p=0.007) in the higher RI group. Among the preoperative laboratory findings of the recipients, the white blood cell count (rWBC) (5,280 vs. 3,890/μL, p=0.029), serum protein level (6.77 vs. 6.44 g/dL, p=0.030) and creatinine level (1.48 vs. 0.88 mg/dL, p=0.035) were significantly higher in the higher RI group. Among the texture and shape parameters, the effective diameter, surface area, $roundness_m$ and compactness1 were significantly lower in the high RI group, while sphericity was significantly higher in the higher RI group (all p<0.05).

The comparisons of the clinical, texture and shape parameters between smaller and larger $eGRWR_{post}$ groups with the cutoff value of 2% are summarized in Tables 3 and 4, respectively.

Table 3. The comparisons of clinical parameters between smaller and larger $eGRWR_{post}$ groups

Variables	**Total (n = 102)**	**Smaller $eGRWR_{post}$ (n = 84)**	**Larger $eGRWR_{post}$ (n = 18)**	**P-value**
Demographics				
Age, donor (years)	30.4 ± 10.4	30.6 ± 10.8	29.7 ± 8.0	0.732
Female sex, donor	26 (25.5%)	21 (25.0%)	5 (27.8%)	0.773
Age, recipient (years)	53.7 ± 7.0	53.6 ± 6.8	54.3 ± 7.9	0.700
Female sex, recipient	22 (21.6%)	19 (22.6%)	3 (16.7%)	0.757
Height, recipient (cm)	165.4 ± 7.1	165.9 ± 7.3	162.8 ± 6.1	0.102
Body weight, recipient (kg)	65.6 ± 10.0	66.7 ± 9.8	60.4 ± 9.5	0.014

BMI, recipient (kg/m^2)	24.0 ± 3.2	24.3 ± 3.2	22.7 ± 3.2	0.073
BSA, recipient (m^2)†	1.732 ± 0.154	1.750 ± 0.150	1.649 ± 0.150	0.011
Clinical features, recipient				
Urgent transplantation	3 (2.9%)	3 (3.6%)	0 (0.0%)	1.000
Underlying HCC	64 (62.7%)	54 (64.3%)	10 (55.6%)	0.487
Pretreatment encephalopathy	21 (20.6%)	15 (17.9%)	6 (33.3%)	0.196
Preop. lab findings, recipient				
WBC (× 10^3/μL)	4.42 ± 2.75	4.24 ± 2.63	5.26 ± 3.21	0.153
Hemoglobin (g/dL)	11.4 ± 2.2	11.5 ± 2.3	11.0 ± 1.6	0.390
Platelet (× 10^3/μL)	82.3 ± 48.8	79.1 ± 43.6	97.3 ± 67.7	0.287
Cholesterol (mg/dL)	111.3 ± 42.5	110.0 ± 43.1	116.8 ± 40.5	0.542
Protein (g/dL)	6.57 ± 0.74	6.52 ± 0.74	6.81 ± 0.72	0.139
Albumin (g/dL)	3.07 ± 0.66	3.09 ± 0.68	2.98 ± 0.54	0.528
Total bilirubin (mg/dL)	5.51 ± 8.11	5.45 ± 8.35	5.76 ± 7.08	0.887
Direct bilirubin (mg/dL)	2.66 ± 4.97	2.37 ± 4.60	4.04 ± 6.56	0.316
Alkaline phosphatase (IU/L)	118.9 ± 82.9	111.2 ± 55.6	155.2 ± 155.1	0.251
AST (IU/L)	66.3 ± 51.6	67.0 ± 51.2	62.7 ± 54.8	0.750
ALT (IU/L)	45.3 ± 34.9	47.5 ± 36.0	35.2 ± 27.7	0.176
GGT (IU/L)	65.1 ± 64.0	66.1 ± 66.7	59.8 ± 48.4	0.745
PT-INR	1.67 ± 0.93	1.69 ± 1.00	1.56 ± 0.52	0.609
Creatinine (mg/dL)	1.11 ± 1.10	1.00 ± 0.49	1.64 ± 2.39	0.270
Sodium (mmol/L)	136.3 ± 6.4	136.2 ± 6.2	136.9 ± 7.7	0.674
MELD score	17.3 ± 9.5	17.1 ± 9.5	18.1 ± 9.4	0.712

Note - $eGRWR_{post}$ = graft-to-recipient weight ratio at postoperative follow-up, BMI = body mass index, BSA = body surface area, WBC = white blood cell, AST = aspartate aminotransferase, ALT = alanine aminotransferase, GGT = gamma-glutamyl transferase, PT-INR = prothrombin time-international normalized ratio, MELD = model for end-stage liver disease.

† BSA was calculated according to Mosteller formula: BSA (m^2) = (Height (cm)*Body weight (kg)/3600)$^{1/2}$

Table 4. The comparisons of texture and shape parameters between smaller and larger $eGRWR_{post}$ groups

Variables	Total (n = 102)	Smaller $eGRWR_{post}$ (n = 84)	Larger $eGRWR_{post}$ (n = 18)	P-value
Liver volume				
LV_{pre} (mL)	781 ± 143	789 ± 141	744 ± 146	0.228
$eGRWR_{pre}$ (%)	1.22 ± 0.28	1.21 ± 0.28	1.26 ± 0.28	0.515
LV_{post} (mL)	1120 ± 237	1055 ± 160	1421 ± 304	< 0.001
$eGRWR_{post}$ (%)	1.73 ± 0.39	1.60 ± 0.23	2.36 ± 0.38	< 0.001
1st order statistics				
Mean attenuation (HU)	106.4 ± 8.7	106.3 ± 8.9	107.2 ± 8.1	0.678
Minimum attenuation (HU)	67.2 ± 9.1	67.7 ± 9.0	64.8 ± 9.6	0.231
Maximum attenuation (HU)	148.9 ± 10.4	148.6 ± 10.3	150.4 ± 10.9	0.497
Standard deviation	8.201 ± 1.266	8.244 ± 1.211	7.999 ± 1.523	0.458
Variance	68.84 ± 19.12	69.42 ± 18.65	66.17 ± 21.56	0.516
Skewness	0.929 ± 0.422	0.954 ± 0.405	0.810 ± 0.492	0.190
Kurtosis	1.833 ± 1.089	1.783 ± 0.979	2.067 ± 1.517	0.317
Entropy	4.866 ± 0.245	4.873 ± 0.232	4.831 ± 0.307	0.515
Homogeneity (× 10^{-3})	9.801 ± 0.909	9.821 ± 0.925	9.712 ± 0.850	0.648
Uniformity (× 10^{-3})	45.68 ± 8.99	45.40 ± 8.35	47.01 ± 11.72	0.493
Energy (× 10^{9})	10.52 ± 2.44	10.52 ± 2.47	10.49 ± 2.34	0.966

Geometric features				
Effective diameter	496.5 ± 45.2	499.1 ± 45.1	484.7 ± 45.1	0.222
Surface area (× 10^3)	89.26 ± 11.04	89.50 ± 10.79	88.15 ± 12.41	0.640
Sphericity	0.769 ± 0.084	0.768 ± 0.081	0.773 ± 0.098	0.834
Discrete compactness	0.938 ± 0.021	0.938 ± 0.019	0.937 ± 0.029	0.840
Roundness$_m$	-0.002 ± 5.675	0.889 ± 5.351	-4.160 ± 5.412	< 0.001
Moment	1.064 ± 0.174	1.061 ± 0.178	1.078 ± 0.161	0.701
Compactness1	219.7 ± 26.3	221.5 ± 26.6	211.0 ± 24.1	0.126
Compactness2	0.098 ± 0.018	0.099 ± 0.018	0.093 ± 0.019	0.182
2nd order statistics (GLCM)				
GLCM ASM (× 10^{-3})	11.91 ± 4.66	11.85 ± 4.31	12.22 ± 6.19	0.762
GLCM IDM	0.597 ± 0.056	0.599 ± 0.056	0.593 ± 0.058	0.699
GLCM contrast	132.0 ± 37.1	128.3 ± 20.7	149.2 ± 75.5	0.258
GLCM entropy	7.732 ± 0.482	7.735 ± 0.464	7.718 ± 0.573	0.893

Note - $eGRWR_{post}$ = estimated graft-to-recipient weight ratio at postoperative follow-up, LV_{pre} = volume of the future graft, $eGRWR_{pre}$ = estimated graft-to-receipient weight ratio before transplantation, LV_{post} = volume of the transplanted liver, GLCM = grey-level co-occurence matrix, ASM = angular second moment, IDM = inverse difference moment.

When compared according to $eGRWR_{post}$, recipient body weight (66.7 kg vs. 60.4 kg, p=0.014) and body surface area (rBSA) (1.750 m^2 vs. 1.649 m^2, p=0.011) were smaller in the larger $eGRWR_{post}$ group. LV_{post} was significantly larger in the larger $eGRWR_{post}$ group (1,055 mL vs. 1,421 mL, p<0.001), while LV_{pre} (789 mL vs. 744 mL, p=0.228) and $eGRWR_{pre}$ (1.21% vs. 1.26%, p=0.515) did not show significant difference between the smaller and larger $eGRWR_{post}$ groups. Among the texture and shape parameters, $roundness_m$

(0.889 vs. -4.160, p<0.001) was the only parameter that was significantly different between the smaller and larger $eGRWR_{post}$ groups.

The results of the linear regression analysis between the RI and clinical, texture and shape parameters are summarized in Tables 5 and 6. Since the rWBC did not satisfy the normality assumption, the analysis for rWBC was performed after log-transformation. LV_{pre} (β=-0.160, 95% CI -0.203 – -0.117, p<0.001) and $eGRWR_{pre}$ (β=-78.553, 95% CI -100.750 – -56.356, p<0.001) showed a significant negative linear association with the RI. Female donors (β=34.313, 95% CI 18.226 – 50.400, p<0.001), log(rWBC) (β=19.207, 95% CI 4.922 – 33.491, p=0.009), serum protein level (β=10.367, 95% CI 0.287 – 20.446, p=0.044) showed a significant positive linear association with the RI, while female recipients (β=-28.301, 95% CI -45.937 – -10.665, p=0.002) showed significant negative association with RI. Among the texture and shape parameters, energy, effective diameter, surface area, $roundness_m$, compactness1 showed a significant negative linear association with the RI, while sphericity and GLCM contrast showed a significant positive linear association with the RI (all p<0.05)

Table 5. Linear regression analysis between RI and clinical parameters

Variables	Estimate	95% CI	P-value
Demographics			
Age, donor (years)	0.286	-0.450 - 1.022	0.443
Female sex, donor	34.313	18.226 - 50.400	< 0.001
Age, recipient (years)	-0.379	-1.468 - 0.711	0.492
Female sex, recipient	-28.301	-45.937 - -10.665	0.002

Height, recipient (cm)	0.877	-0.179 - 1.932	0.103
Body weight, recipient (kg)	0.547	-0.211 - 1.304	0.155
BMI, recipient (kg/m^2)	0.769	-1.600 - 3.139	0.521
BSA, recipient (m^2)†	40.866	-8.063 - 89.795	0.101
Clinical features, recipient			
Urgent transplantation	-16.735	-61.668 - 28.198	0.462
Underlying HCC	0.123	-15.622 - 15.868	0.988
Pretreatment encephalopathy	5.503	-13.292 - 24.298	0.563
Preop. lab findings, recipient			
Log(WBC) (× 10^3/μL)	19.207	4.922 - 33.491	0.009
Hemoglobin (g/dL)	-0.224	-3.736 - 3.288	0.900
Platelet (× 10^3/μL)	0.146	-0.009 - 0.300	0.064
Cholesterol (mg/dL)	-0.005	-0.185 - 0.175	0.959
Protein (g/dL)	10.367	0.287 - 20.446	0.044
Albumin (g/dL)	-0.519	-12.166 - 11.128	0.930
Total bilirubin (mg/dL)	0.356	-0.586 - 1.297	0.455
Direct bilirubin (mg/dL)	0.861	-1.198 - 2.919	0.407
Alkaline phosphatase (IU/L)	0.012	-0.080 - 0.105	0.791
AST (IU/L)	-0.034	-0.182 - 0.114	0.648
ALT (IU/L)	-0.131	-0.349 - 0.087	0.236
GGT (IU/L)	0.049	-0.079 - 0.177	0.446
PT-INR	-0.051	-8.261 - 8.160	0.990
Creatinine (mg/dL)	6.388	-0.424 - 13.201	0.066
Sodium (mmol/L)	-0.186	-1.373 - 1.000	0.756
MELD score	0.313	-0.493 - 1.119	0.443

Note - RI = regeneration index, CI = confidence interval, BMI = body mass index, BSA = body surface area, WBC = white blood cell, AST = aspartate aminotransferase, ALT = alanine aminotransferase, GGT = gamma-glutamyl transferase, PT-INR = prothrombin time-international normalized ratio, MELD = model for end-stage liver disease.

† BSA was calculated according to Mosteller formula: BSA (m^2) = (Height (cm)*Body weight (kg)/3600)$^{1/2}$

Table 6. Linear regression analysis between RI and texture and shape parameters

Variables	Estimate	95% CI	P-value
Liver volume			
LV_{pre} (mL)	-0.160	-0.203 - -0.117	< 0.001
$eGRWR_{pre}$ (%)	-78.553	-100.750 - -56.356	< 0.001
1st order statistics			
Mean attenuation (HU)	0.444	-0.429 - 1.318	0.316
Minimum attenuation (HU)	-0.340	-1.177 - 0.498	0.423
Maximum attenuation (HU)	0.371	-0.360 - 1.103	0.316
Standard deviation	0.501	-5.539 - 6.541	0.870
Variance	0.096	-0.303 - 0.496	0.633
Skewness	-13.002	-30.932 - 4.927	0.153
Kurtosis	2.776	-4.224 - 9.776	0.433
Entropy	3.160	-28.034 - 34.354	0.841
Homogeneity (× 10^{-3})	-5.558	-13.901 - 2.786	0.189
Uniformity (× 10^{-3})	0.000	-0.851 - 0.851	1.000
Energy (× 10^{9})	-3.209	-6.278 - -0.139	0.041
Geometric features			
Effective diameter	-0.521	-0.655 - -0.387	< 0.001
Surface area (× 10^{3})	-1.818	-2.409 - -1.226	< 0.001
Sphericity	114.468	25.882 - 203.054	0.012
Discrete compactness	264.750	-94.633 - 624.132	0.147
$Roundness_m$	-2.682	-3.921 - -1.444	< 0.001
Moment	18.708	-25.115 - 62.529	0.399

Compactness 1	-0.823	-1.064 - 0.583	< 0.001
Compactness 2	-276.173	-689.977 - 137.630	0.189
2nd order statictics (GLCM)			
GLCM ASM (× 10^{-3})	-0.472	-2.112 - 1.168	0.569
GLCM IDM	-130.324	-264.356 - 3.707	0.057
GLCM contrast	0.226	0.025 - 0.427	0.028
GLCM entropy	9.152	-6.621 - 24.925	0.252

Note - RI = regeneration index, CI = confidence interval, LV_{pre} = volume of the future graft, $eGRWR_{pre}$ = estimated graft-to-recipient weight ratio before transplantation, GLCM = grey level co-occurence matrix, ASM = angular second moment, IDM = inverse difference moment.

Prediction model for liver regeneration

The variables with p-value less than 0.2 in the univariate analysis were initially selected for stepwise multivariate linear regression analysis. There was a high correlation between 1) LV_{pre}, effective diameter, surface area and compactness1, 2) recipient body weight and rBSA, and 3) sphericity and discrete compactness. Therefore, variables with the highest statistical significance in each group - effective diameter, rBSA and sphericity were selected, and the others were excluded to avoid multicollinearity. The stepwise multivariate linear regression analysis showed that the effective diameter, $roundness_m$, rBSA, donor sex and log(rWBC) were significantly associated with the RI. The effective diameter (β=-0.367, 95% CI -0.512 – -0.223, p<0.001) and $roundness_m$ (β=-1.827, 95% CI -2.847 – -0.806, p=0.001) had a negative linear association with the RI, while rBSA

(β=47.371, 95% CI -12.061 – 82.681, p=0.009), female donors (β=18.034, 95% CI 3.899 – 32.169, p=0.013) and log(rWBC) (β=12.041, 95% CI 1.423 – 22.658, p=0.027) were positively associated with the RI (Table 7). The regression equation for predicting the RI was as follows: expected RI (%) = 127.020 – 0.367×effective diameter - 1.827×$roundness_m$ + 47.371×rBSA (m^2) + 12.041×log(rWBC) (× 10^3/μL) + 18.034 (if the donor was female). The R-square of the regression equation was 0.522. Representative cases were shown on Figure 5.

Table 7. Multivariate linear regression model for predicting RI

Variables	Estimate	95% CI	P-value
Intercept	127.020	33.523 – 220.516	0.008
Effective diameter	-0.367	-0.512 - -0.223	< 0.001
$Roundness_m$	-1.827	-2.847 - -0.806	0.001
BSA, recipient (m^2)†	47.371	12.061 - 82.681	0.009
Female sex, donor	18.034	3.899 - 32.169	0.013
Log(WBC), recipient (× 10^3/μL)	12.041	1.423 - 22.658	0.027

Note - RI = regeneration index, CI = confidence interval, BSA = body surface area, WBC = white blood cell

† BSA was calculated according to Mosteller formula: BSA (m^2) = (Height (cm)*Body weight (kg)/3600)$^{1/2}$

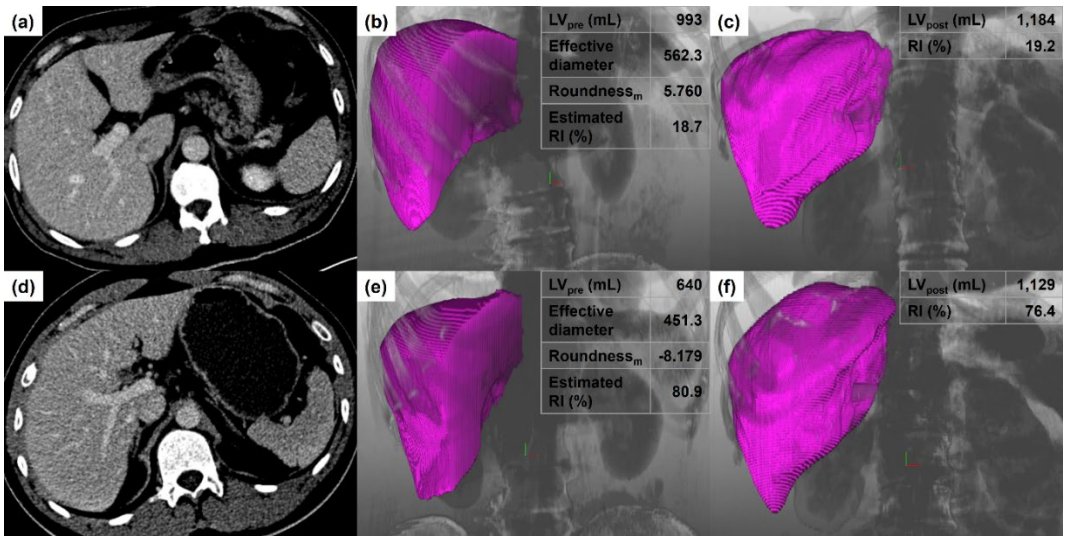

Figure 5. Representative cases of (a-c) lower and (d-f) higher RI groups. (a) A preoperative CT image of a 53-year-old male donor who donated liver to a 60-year-old male recipient who had HBV-related HCC. (b) A future graft was segmented and texture and shape features of the future graft were calculated. Estimated RI was calculated to 18.7% by effective diameter (562.3) and roundness$_m$ (5.760). (c) Postoperative CT of the recipient was taken 12 months after LDLT and the transplanted was segmented. RI was finally calculated to 19.2%. (d) Another preoperative CT image of a 25-year-old male donor who donated liver to a 52-year-old male recipient who had HBV-related HCC. (b) Estimated RI was calculated to 80.9% by effective diameter (451.3) and roundness$_m$ (-8.179) in the same manner. (c) Postoperative CT of the recipient was taken 12 months after LDLT and RI was finally calculated to 76.4%.

Subgroup analysis in the smaller and larger eGRWR$_{pre}$ subgroups

When the donor-recipient pairs were divided into the smaller and larger $eGRWR_{pre}$ subgroups with the cutoff value of 1%, there were 25 and 77 donor-recipient pairs in the smaller and larger $eGRWR_{pre}$ subgroups, respectively. The results of the univariate linear regression analysis between the RI and clinical, texture and shape parameters in the smaller and larger $eGRWR_{pre}$ subgroups are summarized in Tables 8 and 9. LV_{pre}, effective diameter and surface area showed significant negative linear association with the RI in both smaller and larger $eGRWR_{pre}$ subgroups (all $p<0.05$). In the larger $eGRWR_{pre}$ subgroups, $eGRWR_{pre}$, donor and recipient sex, log(rWBC), $roundness_m$, compactness1 and GLCM contrast also showed significant association with the RI (all $p<0.05$), which were similar to the results analyzed in the entire subjects. In the smaller $eGRWR_{pre}$ subgroups, on the other hand, alkaline phosphatase (β=-0.295, 95% CI -0.517 – -0.072, p=0.012) and energy (β=-10.140, 95% CI -17.253 – -3.026, p=0.007) were the only significant parameters other than LV_{pre}, effective diameter and surface area.

Table 8. Linear regression analysis between RI and clinical parameters in the smaller and larger $eGRWR_{pre}$ subgroups.

Variables	**Smaller $eGRWR_{pre}$ (< 1%, n = 25)**		**Larger $eGRWR_{pre}$ (≥ 1%, n = 77)**	
	Estimate (95% CI)	**P-value**	**Estimate (95% CI)**	**P-value**
Demographics				
Age, donor (years)	0.627 (-0.596 - 1.850)	0.300	-0.365 (-1.182 - 0.452)	0.376

Female sex, donor	13.589 (-18.444 - 45.621)	0.389	25.935 (6.092 - 45.777)	0.011
Age, recipient (years)	0.007 (-2.321 - 2.334)	0.995	-0.565 (-1.634 - 0.504)	0.296
Female sex, recipient	-34.089 (-81.609 - 13.431)	0.151	-20.857 (-37.616 - -4.099)	0.015
Height, recipient (cm)	0.782 (-1.460 - 3.025)	0.478	0.365 (-0.708 - 1.439)	0.500
Body weight, recipient (kg)	-1.004 (-3.111 - 1.103)	0.335	0.013 (-0.761 - 0.786)	0.974
BMI, recipient (kg/m^2)	-4.091 (-9.260 - 1.078)	0.115	-0.330 (-2.795 - 2.135)	0.790
BSA, recipient (m^2)†	-40.538 (-182.775 - 101.699)	0.561	5.133 (-44.446 - 54.712)	0.837
Clinical features, recipient				
Urgent transplantation	-	-	-6.258 (-45.070 - 32.554)	0.749
Underlying HCC	-7.296 (-47.584 - 32.993)	0.711	-7.843 (-22.922 - 7.236)	0.303
Pretreatment encephalopathy	14.782 (-28.847 - 58.411)	0.701	6.792 (-11.260 - 24.843)	0.456
Preop. lab findings, recipient				
Log(WBC) (× 10^3/μL)	13.907 (-22.902 - 50.715)	0.442	18.576 (5.281 - 31.872)	0.007
Hemoglobin (g/dL)	-2.746 (-9.870 - 4.378)	0.433	0.560 (-2.944 - 4.064)	0.751
Platelet (× 10^3/μL)	0.158 (-0.144 - 0.460)	0.290	0.123 (-0.033 - 0.280)	0.121
Cholesterol (mg/dL)	0.098 (-0.270 - 0.467)	0.586	-0.011 (-0.190 - 0.169)	0.907

Protein (g/dL)	17.040 (-3.046 - 37.127)	0.093	9.650 (-0.350 - 19.649)	0.058
Albumin (g/dL)	6.665 (-19.099 - 32.429)	0.598	-2.232 (-13.556 - 9.092)	0.696
Total bilirubin (mg/dL)	-0.133 (-2.042 - 1.777)	0.887	0.326 (-0.622 - 1.274)	0.495
Direct bilirubin (mg/dL)	-3.820 (-21.443 - 13.803)	0.645	1.544 (-0.132 - 3.400)	0.101
Alkaline phosphatase (IU/L)	-0.295 (-0.517 - -0.072)	0.012	0.075 (-0.009 - 0.158)	0.080
AST (IU/L)	-0.261 (-0.645 - 0.124)	0.174	0.003 (-0.135 - 0.141)	0.969
ALT (IU/L)	-0.553 (-1.140 - 0.034)	0.064	-0.048 (-0.250 - 0.153)	0.634
GGT (IU/L)	-0.160 (-0.385 - 0.065)	0.152	0.113 (-0.025 - 0.250)	0.106
PT-INR	-6.144 (-22.546 - 10.258)	0.446	0.570 (-8.873 - 7.734)	0.892
Creatinine (mg/dL)	12.139 (-8.840 - 33.118)	0.244	5.787 (-0.384 - 11.958)	0.066
Sodium (mmol/L)	-0.182 (-2.926 - 2.562)	0.892	-0.080 (-1.223 - 1.064)	0.890
MELD score	-0.213 (-1.739 - 1.312)	0.775	0.335 (-0.499 - 1.170)	0.426

Note - RI = regeneration index, $eGRWR_{pre}$ = estimated graft-to-receipient weight ratio before transplantation, CI = confidence interval, BMI = body mass index, BSA = body surface area, WBC = white blood cell, AST = aspartate aminotransferase, ALT = alanine aminotransferase, GGT = gamma-glutamyl transferase, PT-INR = prothrombin time-international normalized ratio, MELD = model for end-stage liver disease.

† BSA was calculated according to Mosteller formula: BSA (m^2) = (Height (cm)*Body weight (kg)/3600)$^{1/2}$

Table 9. Linear regression analysis between RI and texture and shape parameters in the smaller and larger $eGRWR_{pre}$ subgroups

	Smaller $eGRWR_{pre}$ (< 1%, n = 25)		**Larger $eGRWR_{pre}$ (≥ 1%, n = 77)**	
Variables	**Estimate (95% CI)**	**P-value**	**Estimate (95% CI)**	**P-value**
Liver volume				
LV_{pre} (mL)	-0.268 (-0.456 - -0.079)	0.007	-0.116 (-0.171 - -0.061)	< 0.001
$eGRWR_{pre}$ (%)	-154.421 (-326.346 - 17.504)	0.076	-61.404 (-91.046 - -31.762)	< 0.001
1st order statistics				
Mean attenuation (HU)	-1.467 (-4.278 - 1.343)	0.291	0.464 (-0.328 - 1.255)	0.247
Minimum attenuation (HU)	-0.456 (-2.342 - 1.431)	0.622	-0.279 (-1.092 - 0.533)	0.495
Maximum attenuation (HU)	-0.309 (-2.127 - 1.509)	0.728	0.438 (-0.252 - 1.127)	0.210
Standard deviation	1.845 (-8.939 - 12.628)	0.727	-2.596 (-9.028 - 3.836)	0.424
Variance	0.146 (-0.537 - 0.829)	0.663	-0.147 (-0.587 - 0.293)	0.508
Skewness	15.835 (-36.033 - 67.702)	0.534	-10.768 (-27.458 - 5.923)	0.203

Kurtosis	8.985 (-13.786 - 31.756)	0.423	5.587 (-0.758 - 11.932)	0.083
Entropy	1.969 (-58.937 - 62.876)	0.947	-14.548 (-46.801 - 17.705)	0.372
Homogeneity (× 10^{-3})	15.998 (-13.880 - 45.875)	0.279	-5.272 (-12.762 - 2.217)	0.165
Uniformity (× 10^{-3})	0.174 (-1.649 - 1.996)	0.845	0.427 (-0.423 - 1.276)	0.320
Energy (× 10^{9})	-10.140 (-17.253 - -3.026)	0.007	-1.005 (-3.943 - 1.932)	0.498
Geometric features				
Effective diameter	-0.750 (-1.281 - -0.220)	0.008	-0.398 (-0.576 - -0.221)	< 0.001
Surface area (× 10^{3})	-2.553 (-4.495 - -0.610)	0.012	-1.117 (-1.825 - -0.408)	0.002
Sphericity	-46.222 (-308.051 - 215.606)	0.718	52.767 (-38.959 - 144.494)	0.255
Discrete compactness	-352.537 (-1498.509 - 793.436)	0.531	49.429 (-299.574 - 398.433)	0.779
$Roundness_m$	-2.105 (-4.376 - 0.165)	0.068	-2.115 (-3.499 - -0.730)	0.003
Moment	-69.579 (-205.314 - 66.156)	0.300	20.727 (-19.126 - 60.581)	0.304
Compactness1	-0.879 (-1.830 - 0.071)	0.068	-0.605 (-0.906 - -0.305)	< 0.001
Compactness2	172.440 (-783.720 - 1128.600)	0.713	-171.938 (-581.721 - 237.845)	0.406
2nd order statictics (GLCM)				
GLCM ASM (× 10^{-3})	0.335 (-3.345 - 4.014)	0.852	0.495 (-1.155 - 2.145)	0.552

GLCM IDM	-39.917 (-305.846 - 226.012)	0.759	-24.381 (-174.726 - 125.963)	0.748
GLCM contrast	0.473 (-0.335 - 1.282)	0.238	0.197 (0.019 - 0.374)	0.030
GLCM entropy	3.100 (-27.526 - 33.726)	0.836	-2.827 (-19.947 - 14.292)	0.743

Note - RI = regeneration index, $eGRWR_{pre}$ = estimated graft-to-receipient weight ratio before transplantation, CI = confidence interval, LV_{pre} = volume of the future graft, GLCM = grey-level co-occurence matrix, ASM = angular second moment, IDM = inverse difference moment.

The stepwise multivariate linear regression analysis was performed for each subgroup in the same way as for the entire subjects. Among LV_{pre}, effective diameter, surface area and compactness1 that were highly correlated, LV_{pre} and effective diameter were selected for the analysis in the smaller and larger $eGRWR_{pre}$ subgroup, respectively since they showed highest statistical significance in the univariate analysis. In the larger $eGRWR_{pre}$ subgroup, $eGRWR_{pre}$ (β=-64.093, 95% CI -101.270 – -26.917, p=0.001), $roundness_m$ (β=-1.659, 95% CI -3.210 – -0.108, p=0.037) and kurtosis (β=6.748, 95% CI 0.173 – 13.323, p=0.044) were shown to be independently associated with the RI (Table 10). Meanwhile, in the smaller $eGRWR_{pre}$ group, LV_{pre} (β=-0.221, 95% CI -0.410 – -0.033, p=0.024) and energy (β=-10.466, 95% CI -18.736 – -2.796, p=0.016) were the only variables that were independently associated with the RI (Table 11).

Table 10. Multivariate linear regression model for predicting RI in the larger $eGRWR_{pre}$ subgroup.

Variables	Estimate	95% CI	P-value
Intercept	110.363	60.402 - 160.325	< 0.001
$eGRWR_{pre}$ (%)	-64.093	-101.270 - -26.917	0.001
$Roundness_{m}$	-1.659	-3.210 - -0.108	0.037
Kurtosis	6.748	0.173 - 13.323	0.044

Note - RI = regeneration index, $eGRWR_{pre}$ = estimated graft-to-receipient weight ratio before transplantation, CI = confidence interval.

Table 11. Multivariate linear regression model for predicting RI in the smaller $eGRWR_{pre}$ subgroup.

Variables	Estimate	95% CI	P-value
Intercept	325.147	207.578 - 442.716	< 0.001
Energy ($\times 10^9$)	-10.466	-18.736 - -2.196	0.016
LV_{pre} (mL)	-0.221	-0.410 - -0.033	0.024

Note - RI = regeneration index, $eGRWR_{pre}$ = estimated graft-to-receipient weight ratio before transplantation, CI = confidence interval, LV_{pre} = volume of the future graft.

Discussion

The results of our study showed highly variable RIs ranging from -10.5% to 153.9%, which implied that the degree of liver regeneration was highly variable among recipients. The multivariate linear regression analysis showed that roundness_m and effective diameter were significant independent variables for predicting the RI among the texture and shape features, both of which showed significant negative associations with RI. In addition, roundness_m was also shown to be independent predictive variable for predicting the RI in the larger eGRWR_{pre} subgroup.

Roundness and roundness_m were defined in this software as follows:

$$\text{Roundness} = \frac{R_{mean}}{\frac{\sum_{i=1}^{n}|R_i - R_{mean}|}{n} + R_{mean}}, where\ \ R_{mean} = \frac{\sum_{i=1}^{n} R_i}{n}$$

$$\text{Roundness}_m = (Roundness - 0.780) \times 1000,$$

Ri represents the distance between the center of gravity and i^{th} pixel in the boundary, and n means the total number of pixels in the boundary. According to the equation, roundness equals 1 in the sphere and decreases as the shape moves away from the sphere. Thus, our result implies that subtle morphological changes of the future graft, which are difficult to perceive with the human eye but expressed as decreased roundness, affect liver regeneration in the recipient. A variety of morphologic changes occur in diffuse liver diseases, especially in LC [26; 27], which is known to be associated with a poor regeneration rate [28-30]. However, the specific relationship between morphological change related to decreased roundness and histopathology was not identified. Further research is warranted to find histopathological significance of our results.

Effective diameter, which also showed significant negative association with RI, was defined in this software as follows:

$$\text{Effective diameter} = \sqrt{\frac{Volume}{\pi}}$$

Because the effective diameter is proportional to the volume of the liver, our result indicates that the recipients with smaller grafts have higher regeneration rate. This result is consistent with several previous reports that smaller grafts in the recipient regenerate more rapidly and become similar with initially larger grafts [31; 32]. Nevertheless, there is a limitation for downsizing the graft since small grafts (i.e. less than 40% of standard liver volume of the recipients) may be insufficient for meeting the metabolic demand and may lead to lower graft or patient survival [4; 5; 33].

Liver regeneration is critical in recipients to maintain the functional mass of the liver after receiving partial grafts from living donors [20]. Therefore, it is important to predict liver regeneration and establish proper surgical plans before LDLT. However, the process of the liver regeneration is complex and factors affecting the liver regeneration are not yet fully understood [22]. In this reality, our study provides a potential tool for predicting liver regeneration in recipients using CTTA in future grafts. The prediction of liver regeneration using CTTA has advantages in that CTTA provides quantitative data for predicting liver regeneration and does not require additional examination since it uses preoperative CT of the donors, which are routinely performed in a clinical setting before LDLT. In fact, there was a study using CTTA to predict liver regeneration after LDLT in donors [19]. However, donors and recipients have different environments, and the pattern of the liver regeneration was shown to be different between donors and recipients. Grafts

in recipients tend to regenerate rapidly during the early postoperative period, exceeding the standard liver volume then gradually decreasing, while the remnant liver in donors tends to regenerate slowly [34; 35]. Therefore, the CTTA-based prediction model for liver regeneration in recipients can be expected to be different from that in donors, and eventually, different results were obtained. To our knowledge, this is the first study to apply CCTA for predicting liver regeneration in recipients, which can be helpful for adjusting surgical plans by predicting liver regeneration before LDLT.

Interestingly, our results indicated that the rWBC affected liver regeneration in recipients. A considerable portion of the recipients in our study had leukopenia before LDLT (55/102 with rWBC<$4\times10^3/\mu L$), most likely due to liver cirrhosis. Although the precise role of each immune cell subpopulation is still under debate, it is clear that immune cells play a key role in liver regeneration [36]. There was also an animal study in which neutropenic-induced mice showed impaired liver regeneration after partial hepatectomy [37]. Thus, the relation between the rWBC and RI may be related with the regulatory role of immune cells in liver regeneration. The rBSA was also shown to be associated with the RI, which is thought to be because the graft in the recipient tends to eventually regenerate to a size close to the standard liver volume of the recipient [34; 38] which is proportional to the rBSA [39; 40]. Another interesting result was that donor sex was independently associated with liver regeneration in recipients. Although the mean LV_{pre} was significantly smaller in females than in males (678 vs. 816 mL, $p < 0.001$), there may be other reasons for the difference in liver regeneration between donor sex in addition to the graft size since donor sex remained significant after correcting the variable associated with liver volume – the effective diameter. However, we could not find a previous report that demonstrated

relationship between donor sex and liver regeneration in recipients; therefore, further studies may be warranted.

CT texture parameters are not only affected by the lesion characteristics, but also by CT scanners, acquisition parameters and reconstruction methods [41; 42]. Since all donors in our study underwent preoperative CT with the same scanner and the same protocol, we could minimize the variation of the CT texture parameters due to the CT scanners or acquisition parameters and highlight the changes of liver itself. However, it may be difficult to generalize our results directly to the preoperative liver CT scanned with different scanner or protocols. Further studies using different CT scanners or protocols may solidify our results.

Our study has several limitations. First, our study was designed retrospectively with a relatively small number of patients, so there may be some potentially significant variables which did not show statistical significance in our study. Second, we used postoperative follow-up CT scanned at around 1 year after LDLT rather than early postoperative period. Since rapid regeneration of the graft in the recipient is mostly occurred within 2 months after LDLT, our study is thought to reflect the long-term liver regeneration rather than early regeneration immediately after LDLT [34]. Early regeneration may be clinically more important since it is critical for maintaining the basic metabolic functions of the liver after LDLT [20], but this is difficult to analyze in our retrospective study since postoperative follow-up CT is performed for clinical needs and there is no routine clinical protocol for follow-up CT scan after LDLT. Further prospective study may help determine whether the texture features of the graft are associated early regeneration of the graft after LDLT as well as long-term regeneration. Next, although we

established a predictive model using CTTA, the exact related pathophysiology was not fully identified. Further studies identifying the pathophysiology related to the shape feature may solidify our results. Finally, our predictive model was not externally validated due to the lack of donor-recipient pairs satisfying the inclusion criteria for external validation. Thus, it may be difficult to apply our results directly to general population. Nonetheless, our study demonstrates the potential of CTTA for predicting liver regeneration in recipients who undergo LDLT.

In conclusion, the shape feature calculated by CTTA was shown to be independently associated with liver regeneration after LDLT in recipients after adjusting feature associated with liver volumetry – effective diameter. CTTA may be used as a potential tool for predicting liver regeneration in recipient before LDLT using routine preoperative CT and may help with the surgical planning for LDLT.

References

1 Lee S, Moon D, Hwang S et al (2015) Liver transplantation in Korea: past, present, and future. Transplantation proceedings 47:705-708

2 Kim W, Lake J, Smith J et al (2018) OPTN/SRTR 2016 annual data report: liver. American Journal of Transplantation 18:172-253

3 Hashikura Y, Makuuchi M, Kawasaki S et al (1994) Successful living-related partial liver transplantation to an adult patient. The Lancet 343:1233-1234

4 Lo C-M, Fan S-T, Liu C-L et al (1999) Minimum graft size for successful living donor liver transplantation. Transplantation 68:1112-1116

5 Sugawara Y, Makuuchi M, Takayama T et al (2001) Small-for-size grafts in living-related liver transplantation. Journal of the American College of Surgeons 192:510-513

6 Kousoulas L, Becker T, Richter N et al (2011) Living donor liver transplantation: effect of the type of liver graft donation on donor mortality and morbidity. Transplant International 24:251-258

7 Goja S, Yadav SK, Saigal S, Soin AS (2018) Right lobe donor hepatectomy: is it safe? A retrospective study. Transplant International 31:600-609

8 Taner CB, Dayangac M, Akin B et al (2008) Donor safety and remnant liver volume in living donor liver transplantation. Liver Transplantation 14:1174-1179

9 Shi Z-R, Yan L-N, Du C-Y (2012) Donor safety and remnant liver volume in living donor liver transplantation. World journal of gastroenterology: WJG 18:7327

10 Singh AK, Cronin CG, Verma HA et al (2011) Imaging of preoperative liver transplantation in adults: what radiologists should know. Radiographics 31:1017-

1030

11 Davnall F, Yip CS, Ljungqvist G et al (2012) Assessment of tumor heterogeneity: an emerging imaging tool for clinical practice? Insights into imaging 3:573-589

12 Lubner MG, Smith AD, Sandrasegaran K, Sahani DV, Pickhardt PJ (2017) CT texture analysis: definitions, applications, biologic correlates, and challenges. Radiographics 37:1483-1503

13 Bashir U, Siddique MM, Mclean E, Goh V, Cook GJJAJoR (2016) Imaging heterogeneity in lung cancer: techniques, applications, and challenges. American Journal of Roentgenology 207:534-543

14 Bayanati H, Thornhill RE, Souza CA et al (2015) Quantitative CT texture and shape analysis: can it differentiate benign and malignant mediastinal lymph nodes in patients with primary lung cancer? European Radiology 25:480-487

15 Dhara AK, Mukhopadhyay S, Dutta A, Garg M, Khandelwal NJJodi (2016) A combination of shape and texture features for classification of pulmonary nodules in lung CT images. Journal of Digital Imaging 29:466-475

16 Daginawala N, Li B, Buch K et al (2016) Using texture analyses of contrast enhanced CT to assess hepatic fibrosis. European Journal of Radiology, 85:511-517

17 Lubner MG, Malecki K, Kloke J, Ganeshan B, Pickhardt PJJAR (2017) Texture analysis of the liver at MDCT for assessing hepatic fibrosis. Abdominal Radiology 42:2069-2078

18 Simpson AL, Adams LB, Allen PJ et al (2015) Texture analysis of preoperative CT images for prediction of postoperative hepatic insufficiency: a preliminary study.

Journal of the American College of Surgeons 220:339-346

19 Kim J-E, Kim JH, Park SJ, Choi S-Y, Yi N-J, Han JKJAR (2019) Prediction of liver remnant regeneration after living donor liver transplantation using preoperative CT texture analysis. Abdominal Radiology 44:1785-1794

20 Olthoff KM (2003) Hepatic regeneration in living donor liver transplantation. Liver Transplantation 9:S35-S41

21 Lan X, Zhang H, Li H-Y et al (2018) Feasibility of using marginal liver grafts in living donor liver transplantation. World Journal of Gastroenterology 24:2441

22 Taki-Eldin A, Zhou L, Xie H-Y, Zheng S-S (2012) Liver regeneration after liver transplantation. European Surgical Research 48:139-153

23 Cho JY, Suh KS, Kwon CH et al (2005) The hepatic regeneration power of mild steatotic grafts is not impaired in living-donor liver transplantation. Liver Transplantation 11:210-217

24 Cho JY, Suh K-S, Kwon CH, Yi N-J, Lee KU (2006) Mild hepatic steatosis is not a major risk factor for hepatectomy and regenerative power is not impaired. Surgery 139:508-515

25 Kianmanesh R, Piardi T, Tamby E et al (2013) Liver angulometry: a simple method to estimate liver volume and ratios. HPB 15(12):976-984.

26 Ozaki K, Matsui O, Kobayashi S, Minami T, Kitao A, Gabata T (2016) Morphometric changes in liver cirrhosis: aetiological differences correlated with progression. The British Journal of Radiology 89:20150896

27 Ozaki K, Matsui O, Kobayashi S et al (2010) Selective atrophy of the middle hepatic venous drainage area in hepatitis C–related cirrhotic liver: morphometric

study by using multidetector CT. Radiology 257:705-714

28 Nagasue N, Yukaya H, Ogawa Y, Kohno H, Nakamura T (1987) Human liver regeneration after major hepatic resection. A study of normal liver and livers with chronic hepatitis and cirrhosis. Annals of Surgery 206:30

29 Miyazaki S, Takasaki K, Yamamoto M, Tsugita M, Otsubo T (1999) Liver regeneration and restoration of liver function after partial hepatectomy: the relation of fibrosis of the liver parenchyma. Hepato-gastroenterology 46:2919-2924

30 Iguchi T, Sato S, Kouno Y et al (2003) Comparison of Tc-99m-GSA scintigraphy with hepatic fibrosis and regeneration in patients with hepatectomy. Annals of Nuclear Medicine 17:227-233

31 Akamatsu N, Sugawara Y, Tamura S, Imamura H, Kokudo N, Makuuchi M (2006) Regeneration and function of hemiliver graft: right versus left. Surgery 139:765-772

32 Nishizaki T, Ikegami T, Hiroshige S et al (2001) Small graft for living donor liver transplantation. Annals of Surgery 233:575

33 Kiuchi T, Kasahara M, Uryuhara K et al (1999) Impact of graft size mismatching on graft prognosis in liver transplantation from living donors. Transplantation 67:321-327

34 Haga J, Shimazu M, Wakabayashi G et al (2008) Liver regeneration in donors and adult recipients after living donor liver transplantation. Liver Transplantation 14:1718-1724

35 Kamel IR, Erbay N, Warmbrand G, Kruskal J, Pomfret E, Raptopoulos V (2003) Liver regeneration after living adult right lobe transplantation. Abdominal Imaging

28:0053-0057

36 Markose D, Kirkland P, Ramachandran P, Henderson N (2018) Immune cell regulation of liver regeneration and repair. Journal of Immunology and Regenerative Medicine 2:1-10

37 Selzner N, Selzner M, Odermatt B, Tian Y, van Rooijen N, Clavien PA (2003) ICAM-1 triggers liver regeneration through leukocyte recruitment and Kupffer cell–dependent release of TNF-α/IL-6 in mice. Gastroenterology 124:692-700

38 Olthoff KM, Emond JC, Shearon TH et al (2015) Liver regeneration after living donor transplantation: Adult-to-adult living donor liver transplantation cohort study. Liver Transplantation 21:79-88

39 Urata K, Kawasaki S, Matsunami H et al (1995) Calculation of child and adult standard liver volume for liver transplantation. Hepatology 21:1317-1321

40 Heinemann A, Wischhusen F, Püschel K, Rogiers X (1999) Standard liver volume in the Caucasian population. Liver Transplantation and Surgery 5:366-368

41 Mackin D, Fave X, Zhang L et al (2015) Measuring CT scanner variability of radiomics features. Investigative Radiology 50:757

42 Lu L, Ehmke RC, Schwartz LH, Zhao B (2016) Assessing agreement between radiomic features computed for multiple CT imaging settings. PloS one 11:e0166550

요약 (국문초록)

연구 목적

본 연구는 수술 전 간 공여자의 CT를 이용한 미래 이식편의 텍스처 및 형태 분석 및 임상 지표를 이용하여 생체간이식 후 간 수여자의 간 용적 재생 정도를 예측하기 위해 시행되었다.

연구 방법

간 우엽을 이용하여 생체간이식을 시행한 102 쌍의 공여자-수여자 쌍이 후향적으로 본 연구에 포함되었다. 모든 공여자는 수술 전에 동일한 CT 스캐너를 이용하여 간 CT를 시행하였으며, 상용화된 소프트웨어를 이용하여 해당 CT 영상으로부터 미래 이식편이 될 간 우엽을 반자동으로 분할하였다. 이후 분할된 미래 이식편의 용적(V_{pre})을 측정하고 해당 미래 이식편에 대한 텍스처 및 형태 분석을 시행하였다. 모든 수여자는 수술 후 9 - 15개월 후에 추적 관찰 CT를 시행하였으며, 같은 방식으로 이식편을 분할하고 분할된 이식편의 용적(V_{post})을 측정하였다. 계산된 용적을 이용하여 재생 지수(regeneration index, RI)를 다음과 같이 정의하였다: $[(V_{post}-V_{pre})/V_{pre}]\times 100$ (%). 다변량 선형회귀분석을 이용하여 임상 지표, 텍스처 및 형태 분석 관련 변수와 RI 사이의 상관관계를 평가하고 RI를 예측하는 모델을 생성하였다. 또한 수술 전 예측된 이식편대체중비($eGRWR_{pre}$)를 기준으로 나눈 부집단에서도 같은 방식으로 모델을 생성하였다.

연구 결과

평균 RI는 47.5±38.6%였다. 단변수 분석에서 V_{pre}, energy, effective diameter, surface area, sphericity, $roundness_m$, compactness1 및 grey-level co-occurrence matrix

(GLCM) contrast가 RI와 유의한 상관관계를 보였다 ($p<0.05$). 다변수 분석에서는 effective diameter, $roundness_m$과 함께 공여자의 성별, 수여자의 체표면적(rBSA) 및 백혈구 수(rWBC)가 RI의 독립적인 예측인자로 확인되었다. RI를 예측하는 모델은 다음과 같다: RI (%) = 127.020 – 0.367 × effective diameter – 1.827 × $roundness_m$ + 47.371 × rBSA (m^2) + 12.041 × log(rWBC) (× $10^3/\mu L$) + 18.034 (공여자가 여성인 경우). 부집단 분석에서, $eGRWR_{pre}$가 1% 이상인 집단(n=77)에서는 $eGRWR_{pre}$, $roundness_m$ 및 kurtosis가 RI를 예측하는 독립적인 예측인자로 나타났으나 $eGRWR_{pre}$가 1% 미만인 집단(n=25)에서는 energy와 LV_{pre}만이 독립적인 예측인자로 확인되었다.

결론

Effective diameter와 $roundness_m$을 포함한 텍스처 및 형태 분석 관련 변수가 간 재생과 연관되어 있었으며, 수술 전 CT를 이용한 미래 이식편의 텍스처 분석이 생체간이식 후 간 수여자의 간 재생을 예측하는 데 유용할 것으로 보인다.

주요어 : 간, 생체간이식, 간 재생, 컴퓨터 단층 촬영, 텍스처 분석
학 번 : 2018-25218